

# SARS-CoV-2 M<sup>Pro</sup> Protease Variants of Concern Display Altered Viral Substrate and Cell Host Target Galectin-8 Processing but Retain Sensitivity toward Antivirals

Sizhu Amelia Chen, Elena Arutyunova, Jimmy Lu, Muhammad Bashir Khan, Wioletta Rut, Mikolaj Zmudzinski, Shima Shahbaz, Jegan Iyyathurai, Eman W. Moussa, Zoe Turner, Bing Bai, Tess Lamer, James A. Nieman, John C. Vederas, Olivier Julien, Marcin Drag, Shokrollah Elahi, Howard S. Young, and M. Joanne Lemieux\*



Cite This: *ACS Cent. Sci.* 2023, 9, 696–708



Read Online

ACCESS |



Metrics & More

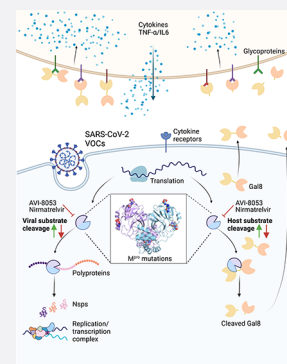


Article Recommendations



Supporting Information

**ABSTRACT:** The main protease of SARS-CoV-2 (M<sup>Pro</sup>) is the most promising drug target against coronaviruses due to its essential role in virus replication. With newly emerging variants there is a concern that mutations in M<sup>Pro</sup> may alter the structural and functional properties of protease and subsequently the potency of existing and potential antivirals. We explored the effect of 31 mutations belonging to 5 variants of concern (VOCs) on catalytic parameters and substrate specificity, which revealed changes in substrate binding and the rate of cleavage of a viral peptide. Crystal structures of 11 M<sup>Pro</sup> mutants provided structural insight into their altered functionality. Additionally, we show M<sup>Pro</sup> mutations influence proteolysis of an immunomodulatory host protein Galectin-8 (Gal-8) and a subsequent significant decrease in cytokine secretion, providing evidence for alterations in the escape of host-antiviral mechanisms. Accordingly, mutations associated with the Gamma VOC and highly virulent Delta VOC resulted in a significant increase in Gal-8 cleavage. Importantly, IC50s of nirmatrelvir (Pfizer) and our irreversible inhibitor AVI-8053 demonstrated no changes in potency for both drugs for all mutants, suggesting M<sup>Pro</sup> will remain a high-priority antiviral drug candidate as SARS-CoV-2 evolves.



## INTRODUCTION

The ongoing COVID-19 pandemic caused by severe acute respiratory syndrome coronavirus 2 (SARS-CoV-2) continues to be a significant threat to global public health.<sup>1,2</sup> SARS-CoV-2 is a positive-sense single-stranded RNA virus with a low genome stability and a high mutation rate.<sup>3–5</sup> The emergence and rapid spread of SARS-CoV-2 variants have posed a greater challenge in the control of the pandemic due to increased transmissibility, disease severity, or resistance toward vaccines and therapies.<sup>6–10</sup> Owing to the potential threats of the variants,<sup>11</sup> Alpha (B.1.1.7), Beta (B.1.351), Gamma (P.1), Delta (B.1.617.2), and most recently Omicron (B.1.1.529) have been classified into variants of concerns (VOCs) by the World Health Organization (WHO).<sup>12</sup> The genomic sequences of new variants are generated and submitted to the Global Initiative on Sharing All Influenza Data (GISAID) with an unprecedented speed, which aids in further understanding of the epidemiology<sup>13</sup> and the distribution of mutations that may lead to changes in viral characteristics.<sup>14</sup>

The SARS-CoV-2 genome encodes two overlapping polyproteins, pp1a and pp1ab, that are proteolytically processed to generate 16 nonstructural proteins (Nsps), followed by four structural proteins that include the envelope (E), membrane (M), nucleocapsid (N), and spike (S) proteins

at the 3' terminus of the genome.<sup>15,16</sup> Multiple mutations occur in various regions of the viral genome.<sup>17</sup> Mutations in the spike protein, which mediates viral entry into human cells (S), is one primary focus of the current research of SARS-CoV-2 variants due to their high impact on infectivity,<sup>18</sup> transmissibility<sup>19</sup> and potential immune escape from antibodies.<sup>20</sup> However, limited studies have examined mutations in other essential viral proteins. Notably, single point mutations found in SARS-CoV-2 variants are also observed in the nsp5 gene, which encodes the viral main protease (M<sup>Pro</sup>, also called 3CLpro).<sup>21</sup> M<sup>Pro</sup> cleaves the polyproteins at 11 positions with a consensus cleavage sequence Leu Gln I (Ser, Ala, Gly) to release nsp's, which are required to assemble the viral replication-transcription complex.<sup>22,23</sup> Previous studies show that SARS-CoV and SARS-CoV-2 M<sup>Pro</sup> share highly similar three-dimensional structures with a 96% sequence identity.<sup>24,25</sup> SARS-CoV-2 M<sup>Pro</sup> is a cysteine protease that forms a dimer

Received: January 11, 2023

Published: March 21, 2023



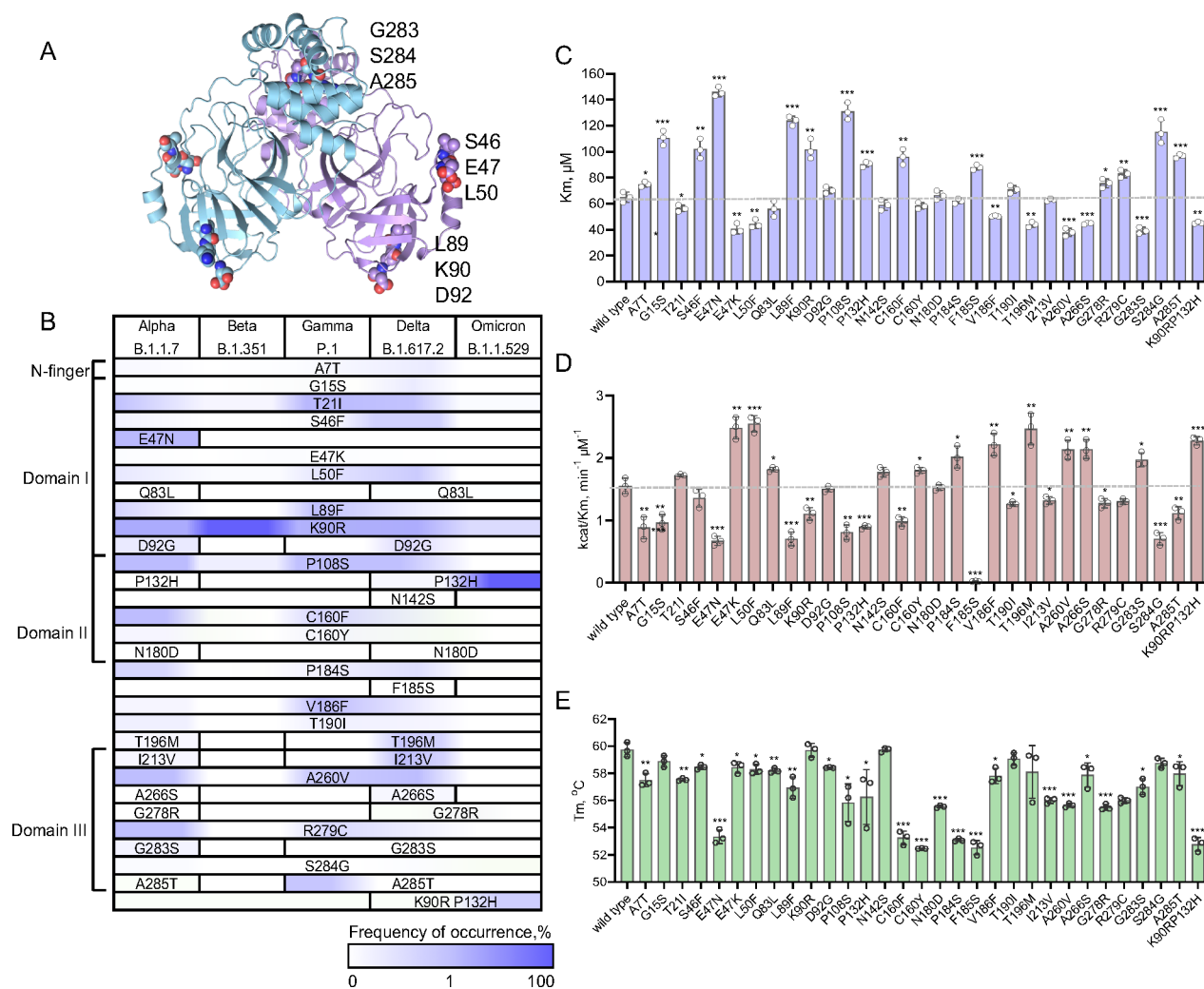


**Figure 1.** Distribution, prevalence, and functional differences of mutations in SARS-CoV-2 M<sup>Pro</sup>. (A) The crystal structure of SARS-CoV-2 M<sup>Pro</sup> dimer (PDB 6WTM) mapping VOC mutations from the GISAID database (<https://gisaid.org>). (B) VOC mutation prevalence was calculated and presented as a heat map. The color gradient of the heatmap is presented in log scale. (C–E) SARS-CoV-2 M<sup>Pro</sup> mutants reveal differences in (C)  $K_M$ , (D) catalytic efficiency ( $k_{cat}/K_M$ ), and (E)  $T_m$  values. \*:  $p < 0.05$  between wild type and the mutants. \*\*:  $p < 0.01$ . \*\*\*:  $p < 0.001$ .

composed of two protomers.<sup>23,25</sup> Each protomer comprises the chymotrypsin and 3C-like peptidase domains I and II (residues 10–99 and 100–182, respectively), with the active site consisting of a Cys145-His41 catalytic dyad located in the cleft between the two antiparallel- $\beta$ -barrel domains. The  $\alpha$ -helical domain III (residues 198–303) linked to domain II by a long loop regulates the dimer formation where dimerization is required for the catalytic activity of M<sup>Pro</sup> to cleave the viral polyproteins.

In addition to the indispensable role in viral replication, SARS-CoV-2 M<sup>Pro</sup> also plays an essential role in escaping antiviral defense by cleaving host cell proteins. During pathogenic infection, type I interferon (INF) controls innate and adaptive immune responses and induces host defense mechanisms by activating the JAK-STAT signaling pathway, leading to interferon-stimulated gene (ISG) responses.<sup>26</sup> M<sup>Pro</sup> of different coronaviruses, including porcine deltacoronavirus,<sup>27,28</sup> porcine epidemic diarrhea virus,<sup>29</sup> and feline infectious peritonitis virus,<sup>30</sup> disrupts the INF-induced pathway by cleaving NF- $\kappa$ B essential modulator (NEMO).

Galactins are essential regulators in host adaptive and innate immune responses.<sup>31</sup> Importantly, recent studies by Pablos et

al. reveal that SARS-CoV-2 M<sup>Pro</sup> contributes to escape host antiviral responses by cleaving host proteins and identified host Galectin-8 (Gal-8) as an M<sup>Pro</sup> substrate.<sup>32</sup> Gal-8 consists of two carbohydrate recognition domains (CRDs) joined by a linker peptide, which binds to glycans on damaged lysosomes or phagosomes upon infections and recruits autophagy adaptors,<sup>33,34</sup> such as NDP52.<sup>35</sup> Pablos et al. showed M<sup>Pro</sup> cleaves Gal-8 at the short linker region, DLQ158↓ST, which dislocates the CRD1 from the CRD2. In the same study it was demonstrated that during SARS-CoV-2 infection, Gal-8 binds to spike glycoprotein, but the Gal-8:NDP52 complex and subsequent autophagy is disrupted upon Gal-8 cleavage by M<sup>Pro</sup>, further demonstrating that proteolytic processing of Gal-8 is an important antiviral mechanism to overcome host defenses allowing SARS-CoV-2 to escape antiviral xenophagy.<sup>32</sup>

Given the critical roles of SARS-CoV-2 M<sup>Pro</sup> in viral replication as well as host immune escape, and the potential vaccine resistance developed by SARS-CoV-2 variants,<sup>36</sup> M<sup>Pro</sup> is an attractive target for drug design to treat COVID-19. The orally administered drug Paxlovid, developed by Pfizer, contains an active component nirmatrelvir, a peptidomimetic

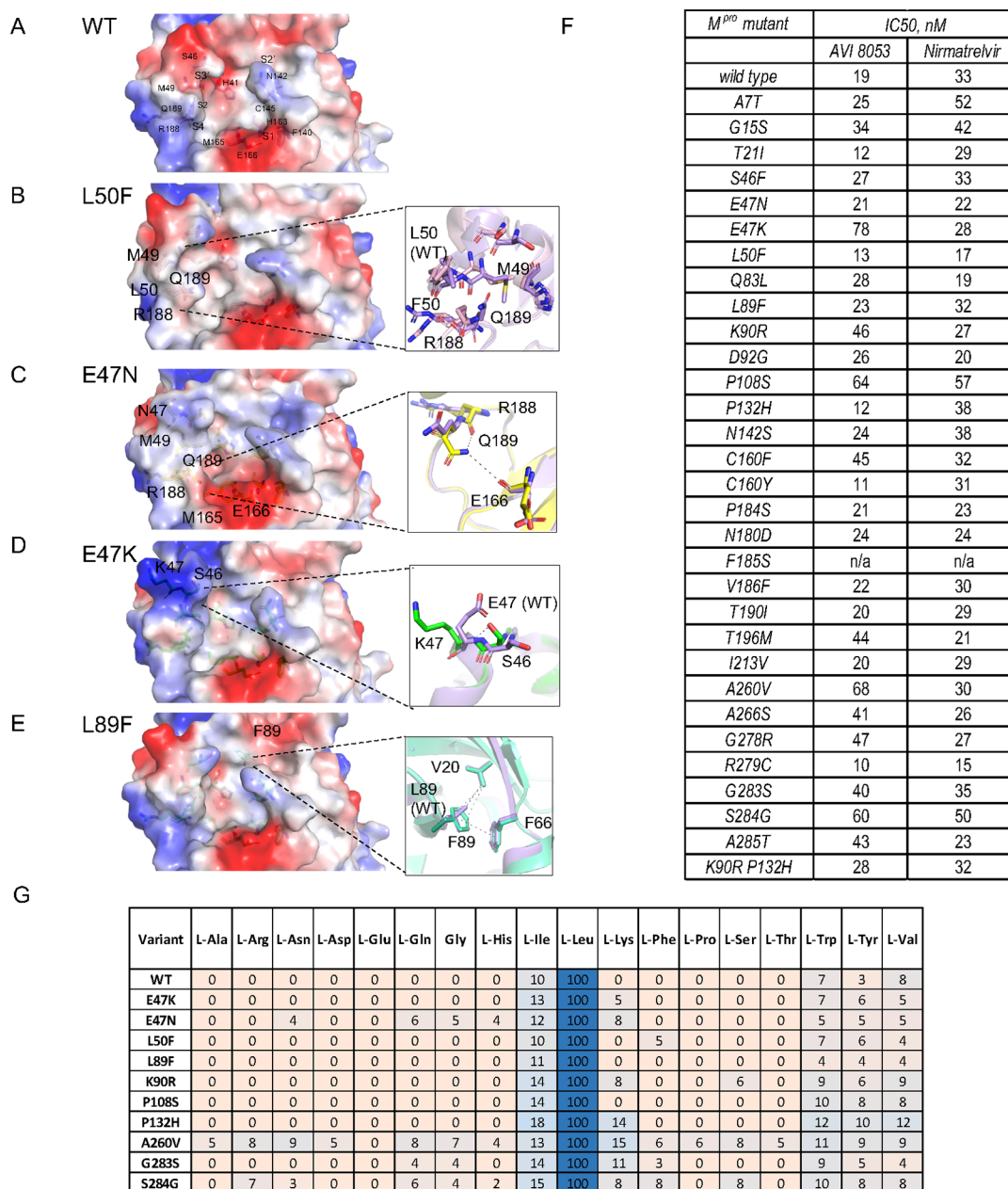


**Figure 2.** Molecular surface representations showing the electrostatic surface potentials of *M<sup>pro</sup>* wild type (A) and the mutants (B–E). Hydrogen bonds and hydrophobic interactions between residues of interest are depicted in the insets. Wild type structure is indicated by purple. (F) *IC<sub>50</sub>* values of *M<sup>pro</sup>* wild type and the mutants for AVI inhibitor AVI-8053 and nirmatrelvir. (G) Substrate specificity profile of SARS-CoV-2 *M<sup>pro</sup>* as presented as heat maps using a substrate library with natural amino acids assessing the P2 position with Ac-Mix-Mix-P2-Gln-ACC.

inhibitor of *M<sup>pro</sup>* with a nitrile warhead covalently binding the catalytic cysteine in the active site,<sup>37</sup> but it also requires a codosing with ritonavir, which inactivates the major human drug-metabolizing enzyme, CYP3A4, to enhance the pharmacokinetics of the *M<sup>pro</sup>* inhibitor. Paxlovid™ was authorized by FDA as the first emergency treatment for COVID-19 in December 2021.<sup>38</sup> Since the start of the pandemic, we have also examined diverse inhibitors that target SARS-CoV-2 *M<sup>pro</sup>*. Our previous study has shown that the feline prodrug, GC376, which is used to treat feline coronavirus infection,<sup>39</sup> was a potent inhibitor for SARS-CoV-2 *M<sup>pro</sup>* in vivo,<sup>23</sup> and its analogs displayed increased drug efficacy and solubility.<sup>40</sup> We also developed novel reversible and irreversible inhibitors with nitrile<sup>41</sup> and  $\alpha$ -acyloxymethylketone warheads,<sup>42</sup> AVI-8059 and

AVI-8053, respectively, that had comparable drug efficacy to nirmatrelvir.

With new variants arising over time, different *M<sup>pro</sup>* mutations may result in changes of protein structure, catalytic activity, and most importantly, the potential therapeutic approach targeting *M<sup>pro</sup>*.<sup>21,43</sup> A recent study has shown that the P108S mutation in SARS-CoV-2 *M<sup>pro</sup>* induced structural perturbation around the substrate-binding region, which led to lower enzymic activity and reduced disease severity in patients infected with the SARS-CoV-2 sublineage (B.1.1.284).<sup>43</sup> As for the more transmissible Omicron variant, it carries a single-point mutation, P132H, in *M<sup>pro</sup>*. The crystal structure of P132H *M<sup>pro</sup>* in complex with GC376 was similar to the wild-type *M<sup>pro</sup>*, and both GC376 and nirmatrelvir remain potent



against P132H M<sup>Pro</sup>.<sup>44</sup> However, additional mutations can still occur as SARS-CoV-2 continues to evolve, potentially influencing the M<sup>Pro</sup> structures, leading to the development of drug resistance to M<sup>Pro</sup> inhibitors.

In this study, we examine the effect of 31 point mutations in nsp5 that occurred from Alpha to more recent Omicron VOCs. We show these mutations influence M<sup>Pro</sup> activity, with some enhancing and others decreasing catalytic efficiency of the protease. Furthermore, substrate specificity is also altered for some mutants. We also assess the influence of M<sup>Pro</sup> mutations on cleavage of host substrate Gal-8 and demonstrate that while cleaved Gal-8 is still able to induce the secretion of TNF $\alpha$ /IL6 cytokines the levels are significantly reduced. Importantly, two inhibitors—nimatrelvir and our novel M<sup>Pro</sup> inhibitor—remain potent against all variants of SARS-CoV-2 M<sup>Pro</sup>. Overall, this study describes important changes in nsp5 over the evolution of the virus that have implications in clinical manifestations.

## RESULTS

**Prevalence of Mutations in Nsp5 in SARS-CoV-2 Variants.** We utilized the GISAID Initiative EpiCoV database (<https://www.gisaid.org/>) to identify and monitor the single point mutations in the nsp5 gene from clinical isolates of different SARS-CoV-2 lineages. The genomes of 5 VOCs were analyzed with the hCoV-19/Wuhan/WIV04/2019 (WIV04) sequence as an official reference sequence. We selected 31 mutations based on the frequency of occurrence as well as the importance for functionality based on location within the protein molecule (Figure 1A,B and Table S1) and grouped them in several hot spots (Figure 1A): clustered near the active site (L50F, E47K, E47N, and S46F), at the end of a beta-sheet behind the active site (D92G, K90R, and L98F), and at the dimer interface (G283S, S284G, and A285T).

Two of the most prevalent mutations in NSP5 are K90R and P132H (Figure 1B and Table S1). K90R appeared in the Alpha VOC with a prevalence of 23.6% and then became a predominant mutation in the Beta VOC (99.9%), with a lower prevalence in Omicron VOC (0.5%), while the P132H mutation became the most frequent in Omicron VOC (99.9%). Other mutations with relatively high occurrence worth noting are E47N, P108S, C160F, A260V (8.7%, 5.3%, 4.1%, and 3.7% in Alpha VOC) and Gamma and Delta VOCs, 16.2% and 21.7% respectively. The frequency of the K90R mutation became very low in Omicron.

We also chose a double mutation, K90R P132H, which appeared in the Delta variant with a very low frequency (0.004%) but became more prevalent in Omicron (0.8%).

**Kinetic Parameters and Structural Alterations in M<sup>Pro</sup> Mutants Found in Five Variants of Concern.** The most significant effect of mutations on proteolytic efficiency of M<sup>Pro</sup> was observed for the residues belonging to Domain I and located near the active site.

L50F is part of the “active site gateway”, a region comprised of two loops L50-Y54 and D187-A191. The mutant exhibited a lower  $K_M$  value, slightly increased  $k_{cat}$ , and subsequently 1.6-fold higher catalytic efficiency compared to the wild type (Figure 1C,D). The L50F crystal structure revealed the loss of charge around the S2 binding site and changes in the orientation of side chains of M49 and R188 residues involved in S2 formation. The S2 site is known to undergo slight structural changes upon binding to Leu in the P2 position,<sup>43,46</sup> and alterations in M49 and R188 side chains may make it more

accessible for the substrate, decreasing the  $K_M$  value (Figure 2A,B inset, Figure S2A,B).

Two substitutions found for the E47 residue (E47N and E47K) had drastically different effects on protease activity—polar Asn had less tolerance, leading to a 2-fold increase in the  $K_M$ , whereas positively charged Lys had the opposite effect on substrate binding, making the enzyme more efficient (Figure 1C,D). The crystal structure of the E47N mutant revealed the change in side chain orientation of amino acids M49, M165, E166, and Q189 involved in the S2, S3, and S4 substrate binding sites resulting in the altering surface charge distribution. Also the side chain of Q189 formed weak hydrogen bonds with the backbones of R188 and E166 residues, which are absent in the wild type structure and could affect the formation of S2, S3, and S4 subsites and the substrate binding ability (Figure 2C inset, Figure S2C). Previous crystal structures of M<sup>Pro</sup> with peptidomimetic inhibitors demonstrated that R188 and E166 residues play significant roles in substrate binding by forming hydrogen bonds with Leu in the P2 position and a residue in the P3 position, respectively.<sup>23,24</sup>

However, in the E47N mutant, these interactions may not be possible explaining the significant increase in the  $K_M$  value. In the structure of the E47K mutant, S2, S3, and S4 binding sites were not altered, but we see that the backbone of K47 forms a strong hydrogen bond with the side chain of S46, which is not found in the wild type structure (Figure 2D inset). S46 is a flexible residue, and its stabilization aids in opening of the active site making it more accessible. Another feature of the E47K mutant worth noting is the drastic change in the charge around the S3' binding site (Figure 2D, Figure S2D).

Charge alteration around the S3' binding site was also observed in the crystal structure of the L89F mutant resulting in a more hydrophobic surface (Figure 2E, Figure S2E). Besides, Phe substitution at position 89 enabled pi-stacking interactions with F66 and hydrophobic interactions with V20, which are not observed in the structure of M<sup>Pro</sup> wild type. These changes may affect the flexibility of the S3' substrate binding pocket (Figure 2E inset), which increased the  $K_M$  value of the L89F mutant 2-fold making the enzyme less efficient (Figure 1C,D).

Another region important for M<sup>Pro</sup> functionality, where a cluster of mutations was identified (A7T, G283S, S2684G, and A285T) is the dimer interface (Figure 1A). Despite the fact that the A7 residue is part of the N-terminus responsible for interaction with the C-terminal domain of second monomer,<sup>25</sup> and threonine substitution changed its hydrophobicity, we observe only a mild effect of this mutation on activity of protease, reducing the efficiency 1.5 times (Figure 1C,D). The crystal structure also revealed no significant changes in the area of the active site, except for the orientation of side chains of N142 rotating toward the catalytic dyad as well as M49 and R188, the residues important for the interaction with Leu in the P2 position and making S2 site less charged (Figure S2F).

C-terminal region mutations involved in dimerization—S284G and A285T—decreased the catalytic efficiency 2 and 1.4 times respectively, whereas G283S substitution was well tolerated (Figure 1C,D). The crystal structures of G283S and S284G did not result in any interesting changes with the exception of a small charge alteration around the S2 site (Figure S2G,H).

The mutants with high prevalence—K90R (99.8% in Beta variant), T21I (9.6% in Gamma), or P132H (99.9% in Omicron)—resulted in no changes in catalytic efficiency with

the exclusion of V186F (7.2% in the Gamma variant) and A260V (3.7% in Alpha and 5% in Delta variants)—these mutations rendered protease 1.5 times more efficient (Figure 1C,D). It is worth noting that for most M<sup>Pro</sup> variants the affected parameter was  $K_M$ , suggesting that mutations altered the substrate binding rather than catalysis itself. Crystal structures of K90R, P132H, T190I and A260V also showed no significant changes, which is consistent with the previously reported structure of Omicron M<sup>Pro</sup> (Figure S2I–L). Interestingly, the catalytic efficiency for the double mutant K90, P132H showed a higher activity revealing a synergistic effect.

Of notable interest was a rare F185S mutation identified in a clinical isolate that had a drastic effect on activity with a 30-fold decrease of turnover rate (Figure 1C,D). F185 is located at the base of the D187–A191 loop, which is a part of the “active site gateway” region. The residues on this loop are involved in forming S2 and S4 substrate binding pockets. F185 forms several interactions, which hold the loop together, pi stacking interaction with P184, and hydrophobic interactions with A194 and with A173, which are parts of the beta-sheet close to the active site. All interactions F185 is involved in are at the same plane and aid in stabilizing the loop (Figure S3B). B-factors of that region confirm that the base of the loop where F185 is located is very rigid, whereas the tip is flexible. One can predict that Ser substitution would result in a loss of important hydrophobic interactions and destabilization of that region. Size exclusion chromatography of SARS-CoV-2 M<sup>Pro</sup> F185S revealed a shift in retention volume with calculated MW of the protein of 49 kDa, suggesting that the mutant exists in a monomeric form, but based on Stokes radius it may have an altered shape of the molecule (Figure S4).

**Differential Scanning Fluorimetry (DSF) Reveals the Differences in Stability of M<sup>Pro</sup> Molecule Variants.** M<sup>Pro</sup> is a stable protein with a  $T_m$  of 59.7 °C, and most mutations had a moderate destabilizing effect on the protease structure (Figure 1E).

The most vulnerable region in the protease molecule where mutations had a significant destabilizing effect was a region in Domain II. We observed a −7 °C shift for C160F, C160Y, and P184S, −4 °C for N180D, −7 °C for F185S, and −2 °C for V186F. C160 is located on a  $\beta$  sheet and forms a hydrophobic interaction with F112, which is located on the antiparallel  $\beta$  sheet. B factors derived from the structure of the wild type indicate that the whole region is very rigid, and one can predict that any perturbations in that area would cause destabilization in protein molecules (Figure S3C). The mutations involved in dimerization—A7T, G283S, S284G, and A285T—exhibited 2 degrees lower  $T_m$ .

The loss of proline at positions 108 and 132 affected the stability of the protein molecule as well and resulted in more significant  $T_m$  changes (−3.9 °C for P108S and −3.5 °C for P132H). Interestingly, we also observed a significant decrease of  $T_m$  for double mutant, K90R P132H (−6.9 °C), whereas the single mutations did not cause changes in thermal stability.

**M<sup>Pro</sup> Inhibitors - Nirmatrelvir and AVI-8053 - Remain Potent against the Variants.** Two peptidomimetic inhibitors against M<sup>Pro</sup> variants, nirmatrelvir (PF-07321332), a component of Paxlovid (Pfizer) and AVI-8053, an irreversible inhibitor with an acyloxymethylketone (AMK) warhead,<sup>42</sup> developed by the Li Ka Shing Applied Virology Institute at the University of Alberta, were tested against 31 M<sup>Pro</sup> mutants. We performed the inhibitory studies and confirmed that all variants

were inhibited by both drugs with nanomolar IC<sub>50</sub> values (Figure 2F), confirming the potency of existing antivirals against VOCs in vitro.

**Mutations in M<sup>Pro</sup> Change Protease Substrate Specificity.** The crystal structures of several variants revealed the changes in side chains orientations of residues in the active site comprising substrate binding pockets, especially S2 and S4, which might lead to altered amino acids preferences. Accordingly, changes in  $K_M$  values for most of variants were observed (Figure 1C), indicating alterations in a mode of substrate binding.

To reveal if mutations caused changes in M<sup>Pro</sup> substrate preferences we chose 10 mutants with the most significant differences in  $K_M$  values and deployed a Hybrid Combinatorial Substrate Library (HyCoSuL) approach.<sup>47</sup> The library consisted of three sublibraries (P2, P3, and P4) of tetrapeptides with two fixed positions: one of each was glutamine at P1 position, as a key feature of SARS-CoV and SARS-CoV-2 main proteases is their ability to cleave the peptide bond after Gln, and two varied positions containing an equimolar mixture of 19 amino acids. P2, P3, or P4 positions in 3 sublibraries correspondingly were represented by 19 natural and over 100 unnatural amino acids. At the C-terminus, an 7-amino-4-carbamoylmethylcoumarin (ACC) fluorescent tag was attached at the P1' position to monitor the cleavage reaction.

The library screen revealed that some variants gained or lost the ability to accommodate certain amino acids in substrate binding pockets (Figure 2G, Figure S5). As it was demonstrated before, Leu is the most preferred amino acid at the P2 position with very low ( $\leq 10\%$ ) activity for other mostly hydrophobic natural amino acids, such as L-Ile and L-Val. However, we observed that the Omicron (P132H) variant as well as variants with mutations close to or at the dimer interface (A260V, G283S, and S284G) permitted charged L-Lys and had an increased activity toward L-Trp and L-Tyr (Figure 2G). Among all mutants A260V was the most promiscuous at this position—allowing almost all amino acids, even L-Pro with low activity though, which is a striking difference compared to the wild type. We observed the same trend with A260V for unnatural amino acids, with this variant becoming the most permissive in comparison to the wild type (Figure S6).

The specificity for the P3 position did not change significantly for most of the variants (Figure S5). All of them as well as the wild type preferred hydrophobic and positively charged amino acids—with L-Lys, L-Arg, L-Val, and L-Thr having the highest activity. Interestingly, many of the variants lost the ability to cleave the substrate with L-Gln and L-His at the P3 position. As described previously, the S3 pocket is not well-defined in the M<sup>Pro</sup> molecule leading to a broad substrate specificity profile for both natural and unnatural amino acids.

The P4 position is permissive as well with a highest preference for L-Ala and L-Val for the wild type (Figure S5). Most of the variants resulted in either the same or lower activity, and some lost the ability to cleave certain amino acids, like L-Ile, L-Pro, and the non-natural amino acids D-Phe,  $\beta$ -Ala, and L-Agb.

**M<sup>Pro</sup> Cleaves Host Protein Gal-8 at Multiple Sites.** M<sup>Pro</sup> plays an important role in viral infection not only because of its essential function for viral replication but also because of interacting directly with host proteins, as it has been reported recently.<sup>32</sup> We sought to study the cleavage of Gal-8, one of the

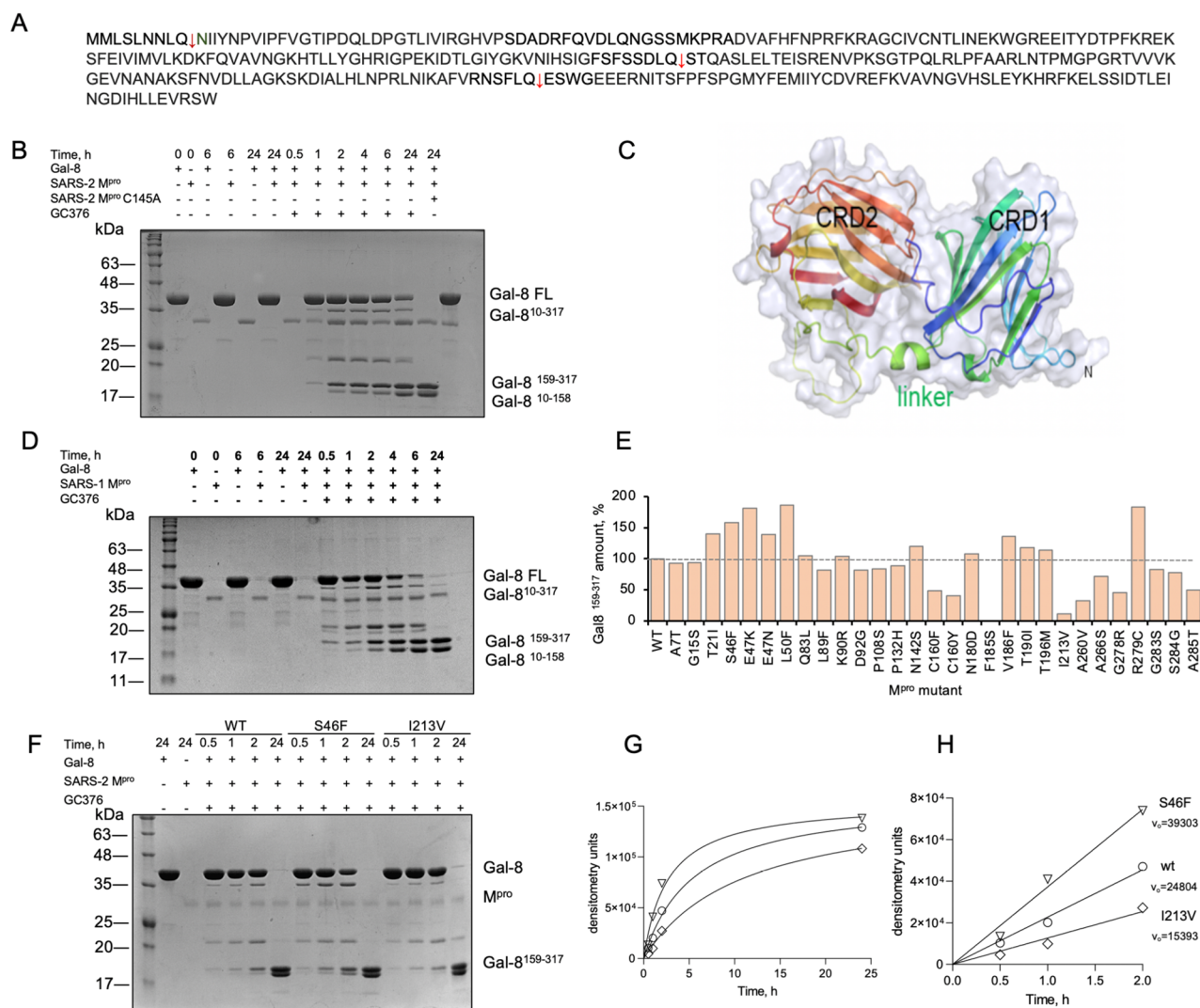


**Figure 3.** Cleavage of host cell substrate Gal-8 by M<sup>Pro</sup> from SARS-CoV-2 variants and SARS-CoV-1. (A) The sequence of Gal-8. The arrows indicate the cleavage sites for viral proteases. (B) SDS-PAGE-based time-course of Gal-8 cleavage by SARS-CoV-2 M<sup>Pro</sup>. Gal-8 was incubated with the protease at 37 °C, and the reaction was stopped at specific time points with M<sup>Pro</sup> inhibitor, GC376. (C) Structural model of Gal-8. CRD: carbohydrate recognition domain. (D) The time course of Gal-8 cleavage by SARS-CoV-1. (E) Gal-8 was cleaved by wild type and M<sup>Pro</sup> mutants. Densitometry analysis of the generated Gal-8<sup>159–317</sup> product in percent in comparison to Gal-8 cleavage by the wild type. (F) SDS-PAGE gel of the time course of Gal-8 cleavage by M<sup>Pro</sup> wild type, M<sup>Pro</sup> S46F, and M<sup>Pro</sup> I213V. (G) The dependence of Gal-8<sup>159–317</sup> band intensities represented in densitometry units on time. (H) The linear part of graph G was used to calculate the initial velocities ( $v_0$ ) of cleavage reactions. The labels are identical on both graphs.

M<sup>Pro</sup> host substrates, in more detail and reveal how mutations in viral protease affect its processing.

Gal-8 was recombinantly expressed in *Escherichia coli*, purified, and incubated with M<sup>Pro</sup>, and the cleavage was detected by the end point SDS-PAGE-based assay and mass spectrometry (Figure S7). The time course of M<sup>Pro</sup> cleavage of Gal-8 revealed that the proteolysis occurs at several sites at the same time with some sites being more accessible than others and some cleavage products being transient (Figure 3A,B). Mass spectrometry analysis identified three sites of M<sup>Pro</sup> scission, NLQ9↓NI, DLQ158↓ST, and FLQ246↓ES, where the DLQ158↓ST site (Figure S7), that was identified previously,<sup>32</sup> is located in the linker region between two carbohydrate recognition domains (Figure 3C). We observed that M<sup>Pro</sup> first cuts Gal-8 at Q9 and Q158 sites, producing Gal-8<sup>10–317</sup> and Gal-8<sup>159–317</sup> cleavage products (34.8 and 17.9 kDa bands respectively). However, after 6 h the Gal-8 10–317 band

disappears after being cut again at the Q158 site resulting in the Gal-8<sup>10–158</sup> product (16.8 kDa). The band at 21 kDa represents the intermediate product of cleavage events at Q246, which then was cut further possibly at Q158, resulting in smaller fragments. Thus, incubation of M<sup>Pro</sup> with Gal-8 for 24 h produced two stable cleavage products: Gal-8<sup>159–317</sup> (17.9 kDa) and Gal-8<sup>10–158</sup> (16.8 kDa).

Since SARS-CoV-2 M<sup>Pro</sup> shares 96% identity in amino acid sequence with SARS-CoV M<sup>Pro</sup> and both enzymes have similar substrate preferences, we were interested to assess if Gal-8 was also a substrate for SARS-CoV M<sup>Pro</sup>. We tested the cleavage of Gal-8 by SARS-CoV M<sup>Pro</sup> using the same approach as for SARS-CoV-2 protease and revealed that the cleavage pattern and the rate of proteolysis were very similar (Figure 3D).

Gal-8 belongs to the tandem-repeat-type subclass of the galectin family, the same as galectin-9 (Gal-9), which also consists of two carbohydrate recognition domains joined by a



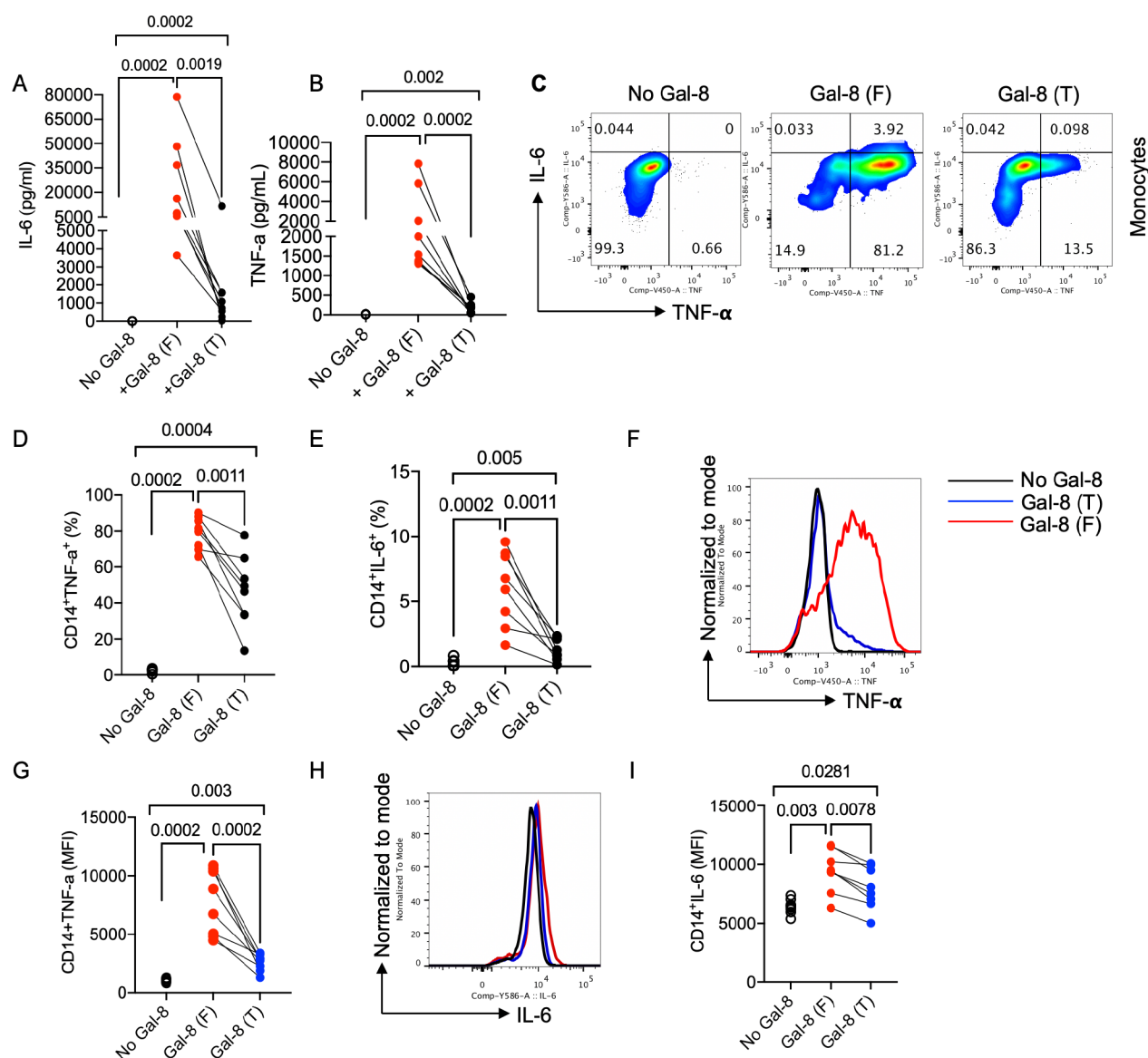


**Figure 4.** (A) Quantification of IL-6 and (B) TNF- $\alpha$  in culture supernatants following stimulation with the full length (F) or the truncated version of Gal-8 (T), consisting of Gal-8<sup>10–158</sup> and Gal-8<sup>159–317</sup>, as measured by ELISA. (C) Representative flow cytometry plots, (D) cumulative data of percentages of TNF- $\alpha$ , and (E) percentages of IL-6 expressing cells among CD14<sup>+</sup> monocytes. (F) Representative histogram plots, and (G) cumulative data of the mean fluorescence intensity (MFI) of TNF- $\alpha$  in CD14<sup>+</sup> cells either unstimulated (No Gal-8) or treated with Gal-8 (F) and Gal-8 (T). (H) Representative histogram plots and (I) cumulative data of the mean fluorescence intensity (MFI) of IL-6 in CD14<sup>+</sup> cells either unstimulated (No Gal-8) or treated with Gal-8 (F) and Gal-8 (T). Each dot represents data from an individual human study subject.

linker peptide. The sequence of Gal-9 has two distinct recognition motifs for M<sup>Pro</sup> – Gln in P1 and Leu in P2 positions. Therefore, it was logical to assume that Gal-9 might also be a substrate for M<sup>Pro</sup> protease. To test this hypothesis, Gal-9 was recombinantly expressed in *E. coli* and purified, and an M<sup>Pro</sup> cleavage assay was performed under the same conditions as for Gal-8. However, we did not detect any cleavage products after 24 h of proteolytic reaction, indicating that Gal-9 is not a substrate of SARS-CoV-2 M<sup>Pro</sup> (Figure S8).

**The Cleavage of Gal-8 by M<sup>Pro</sup> Variants.** The time course of Gal-8 proteolysis by M<sup>Pro</sup> demonstrated that Q158 was the most accessible cleavage site, and Gal-8<sup>159–317</sup> product was detectable after 30 min of cleavage and remained stable for at least 24 h. The dependence of Gal-8<sup>159–317</sup> band formation on time, assessed by densitometry, showed a linear relationship within 2 h (Figure S9A). Therefore, to compare the proteolytic

efficiency of variants the intensities of Gal-8<sup>159–317</sup> bands after 2 h of Gal-8 cleavage by mutants were assessed by densitometry analysis.

The most significant increase of the Gal-8 cleavage rate was observed for the variants with mutations around the active site: S46F, E47K, E47N, L50F, N142S, V186F, and R279C; the lowest activity was demonstrated by the I213V mutant and also F185S, consistent with the previous observations (Figure 3E, Figure S9C). The more detailed time course analysis of two mutants with highest (S46F) and lowest (I213V) activity confirmed the differences in cleavage rates resulting in a 1.5 times increase for S46F and 1.6 times decrease for I213V (Figure 3G,H). The mutations that affected the protein stability (C160F, C160Y, and F185A) demonstrated a significant decrease in activity, highlighting the importance of that region for M<sup>Pro</sup> functionality.

The cleavage of Gal-8 by M<sup>Pro</sup> may lead to several consequences, one of which is the alteration or loss of Gal-8 functionality. Pablos et al. in a recent study demonstrated that the cleavage event at Q158 resulted in a loss of hemagglutination activity of Gal-8, which it possesses due to its bivalent carbohydrate binding capacity.<sup>32</sup> Here we aimed to determine if Gal-8 proteolysis by M<sup>Pro</sup> had an effect on its immune regulatory activity and cytokines secretion, given the fact that cytokines play essential roles in acute and chronic viral infections which can have beneficial effects during viral clearance.

**The Cleavage of Gal-8 by M<sup>Pro</sup> Affects Its Immunomodulatory Activity.** To assess if cleaved Gal-8 was able to demonstrate immune regulatory properties, FL-Gal-8 was incubated with M<sup>Pro</sup> overnight at 37 °C, and the protein sample was subjected to size-exclusion chromatography where Gal-8<sup>159–317</sup> and Gal-8<sup>10–158</sup> products were separated from FL-Gal-8 and M<sup>Pro</sup>. Following this, human peripheral blood mononuclear cells (PBMCs) were cultured in the absence or presence of either FL-Gal-8 or Gal-8<sup>159–317</sup> and Gal-8<sup>10–158</sup> samples (1 μg/mL) overnight. We found that both samples of Gal-8 enhanced TNF-α and IL-6 production in the culture supernatants as measured by ELISA (Figure 4A,B). However, the truncated Gal-8 displayed less pronounced immunomodulatory effects compared to the FL-Gal-8 (Figure 4A,B).

To identify Gal-8 target cells, we subjected PBMCs to further analysis by flow cytometry. These studies revealed that 6 h treatment of PBMCs with both samples of Gal-8 significantly increased the percentages of TNF-α/IL-6 expressing cells among CD14+ monocytes in vitro (Figure 4C–E). We found that both full length and truncated forms of Gal-8 not only increased the frequency of TNF-α/IL-6 expressing monocytes but also elevated the intensity of TNF-α (Figure 4F,G) and IL-6 expression cells among these monocytes (Figure 4H,I). Nevertheless, the truncated version of Gal-8 demonstrated significantly less prominent stimulatory effects on monocytes than the full length (Figure 4C–I).

Moreover, we observed that Gal-8 exhibited a similar effect on B cells (CD19+ cells). As shown in Figure 5A–C, either the full or truncated version of Gal-8 significantly increased the

proportion of TNF-α/IL-6 expressing cells among B cells. Similar to monocytes, the full length of Gal-8 had a more pronounced stimulatory effect on B cells than its truncated version (Figure 5A). However, neither FL nor truncated Gal-8 had any stimulatory effects on both CD4+ and CD8+ T cells in terms of cytokine production (data not shown).

Together the data suggest Gal-8 cleavage will have alterations in host immune response as a result of compromised/impaired cytokine stimulation. Importantly, we do note that increased Gal-8 cleavage was observed in M<sup>Pro</sup> mutations T21I, S46F, E47K and L50F and R279C found in the Delta SARS-CoV-2 VOC (Figure 3E), which has been linked to IFN suppression and higher virulence.<sup>48</sup> In clinical samples, a low production of IFN-γ was associated with more severe cases of COVID-19,<sup>49</sup> and accordingly the Delta VOC is able to produce high viral loads and increased transmission compared to other VOCs.<sup>50,51</sup>

## DISCUSSION

Understanding the pathophysiology of COVID-19 still remains a high priority, especially in the light of newly emerging VOCs. Every discovered variant presents a potential risk of possible clinical implications due to alterations and newly acquired properties in viral components leading to increased transmissibility and/or higher replication rate. This may result in resistance to existing medications or inhibitors under development. Therefore, tracing the mutations occurring in SARS-CoV-2 viral components is essential to ensure the efficacy of potential antivirals.

In this study we analyzed 31 mutations of M<sup>Pro</sup> found in 5 VOCs of SARS-CoV-2. We identified hot spots that had an effect on protease functionality and structural integrity. The hot spots were located around or in close proximity to the active site or at the dimer interface—the region involved in allosteric regulation of M<sup>Pro</sup> activity. Interestingly, previous studies of M<sup>Pro</sup> from SARS-CoV and SARS-CoV-2 particularly demonstrated the importance of long-range interaction for protein structure and function where even a single point mutation might cause a drastic effect for protease function.<sup>25,52–54</sup> However, since we selected mutations found in sequences of clinical isolates and taking into account that M<sup>Pro</sup> function is critical for virus life cycle, we did not expect to find mutations that would cause a significant negative effect on protease activity.

We employed crystallographic structural analysis together with a high fidelity FRET activity assay as described previously by our group to assess the functional and structural changes in M<sup>Pro</sup> mutants.<sup>23,55</sup> The catalytic parameters for most substitutions were not significantly altered with the maximum level of change of 1.7-fold for catalytic efficiency and 2-fold for  $K_M$  values. These findings were not surprising, given the recent study demonstrating that most of the residues, including those that form substrate binding pockets, were able to tolerate quite a bit of variability while maintaining functionality and structural integrity.<sup>56,57</sup> We observe the highest level of conformational plasticity around the S2' and S3' binding pockets with N142 and S46 being the most flexible residues within the structures we solved. Multiple rotamers of N142 were also observed in previous studies.<sup>57,58</sup> N142 is known to have an important role in substrate binding and in binding of several tested inhibitors.<sup>24,59</sup> The flexible side chain of N142 extends over the S1 subsite, forming van der Waals interactions with Gln in the P1 position.<sup>58</sup> In several crystal structures of

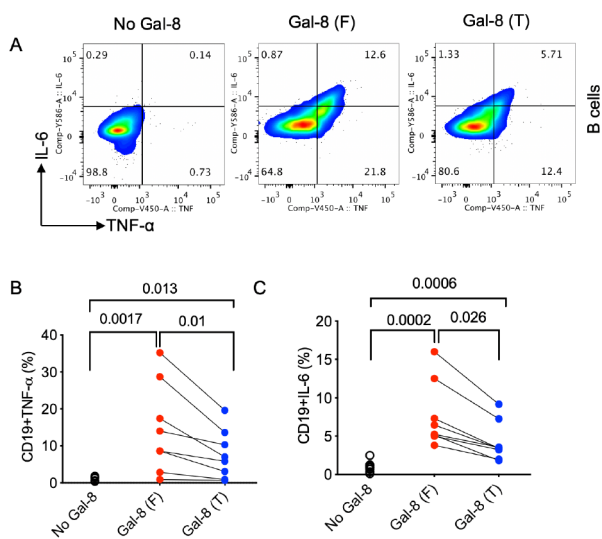


**Figure 5.** (A) Representative flow cytometry plots, (B) cumulative data of percentages of TNF-α, and (C) percentages of IL-6 expressing cells among CD19+ B cells.



M<sup>Pro</sup> with inhibitors, N142 forms hydrogen bonds with water in the active site, stabilizing the bound inhibitor.<sup>24,59</sup> The plasticity of N142 may enhance the binding of Gln which contributes to the conserved feature of M<sup>Pro</sup> cleavage sites.

Also, we observed that the charge distribution in the active site changes quite dramatically even upon a single substitution especially around the S3' and S2 binding pockets. This might explain why with most mutants we see the changes in binding affinities and not the  $k_{cat}$  values. The active site of M<sup>Pro</sup> is unique because it has a natural ability of being malleable enough to accommodate 11 similar yet slightly different cleavage sequences of the viral polypeptide. Several mutations we explored (L50F and E47K/N) were located in close proximity to important elements of the active site and significantly changed the surface charge and orientation of surrounding residues, which were involved in S2, S3', and S4 pockets. The S2 subsite has a preference for Leu but also the plasticity to accommodate Phe as P2 in the 11 endogenous cleavage sequences.<sup>60</sup> Crystal structures of apo M<sup>Pro</sup> reveal that S2 subsite adopts a more open conformation in the empty active site. Upon the binding of Leu in the P2 position, the side chains of M49 and Q189 are redirected, inducing conformational changes in the S2 subsite. L50F and E47N are the mutants that cause the most profound changes in S2 (Figure 2B,C). L50 is located at the surface of the active site, which might contribute to the entrance of substrate binding groove with an open conformation.<sup>57</sup> The substitution of leucine with a bulkier aromatic phenylalanine resulted in a wider open S2 pocket compared to the wild type. Meanwhile M49, M16S, and Q189 are positioned to form additional hydrogen bonds to narrow S2 in the E47N active site. The conformational changes of S2 in structures of apo M<sup>Pro</sup> mutants might lead to sufficient or insufficient binding of substrates indicated by the 3.5-fold difference in  $K_M$  values of L50F and E47N. Despite this, the changes in catalytic parameters were not significant compared to the wild type (Figure 1C,D).

Another group of mutations of interest was located at the dimer interface (Figure 1A). M<sup>Pro</sup> has an allosterically regulated correlation between dimerization and catalysis, demonstrated by the effect of mutating residues involved in dimerization on activity.<sup>52,61,62</sup> However, the apo-structures of the corresponding mutants did not reveal any significant structural changes. Activity assays also did not result in functional consequences.

To further assess if the structural plasticity of the active site of M<sup>Pro</sup> might be affected by mutations, we performed substrate specificity studies. Because M<sup>Pro</sup> recognizes diverse sequences with high specificity, it is thought that substrate recognition is defined by a certain shape that the protease is able to accommodate and not by the amino acid sequence itself.<sup>57</sup> This substrate-envelope hypothesis has also been studied for other viral proteases, including HIV-1 and HCV NS3/4 A proteases.<sup>63–65</sup> Since the structures of several mutants revealed altered orientations of side chains of residues involved in substrate binding pockets and reorganization of hydrogen bond networking around the active site, the M<sup>Pro</sup> ability to recognize certain amino acids could be affected as well. The HyCoSuL approach demonstrated that several mutants indeed had an altered specificity (Figure 2G). The most interesting changes we observed were C-terminus mutants A260V and S284G that became more permissive at the P2 position. The most preferred amino acid in this position is Leu for the wild type, but other hydrophobic residues can be accommodated for the mutants, however with lower activity.

The A260V mutant displayed activity with almost all natural amino acids at P2. Looking at the structures of S284G and A260V mutants, we noticed that the S2 binding pocket and the area around it have lost negative charge in both cases (Figure S2D,L). This might explain the difference in specificity in that region. The dimer interface consisting of the N-finger and C-terminal helix plays a major role in allosteric communication in the M<sup>Pro</sup> dimer.<sup>66</sup> Dimerization or dimer packing can influence the stabilization of both the active site and the protein; therefore, apo-structures may lack distinctive conformational changes to explore the substrate specificity of C-terminal mutants. Further study could assess the distal regions by solving and comparing the ligand-bound crystal structures.

Viral proteins are evolutionary evolved to be multifunctional, and the promiscuous nature of substrate specificity of M<sup>Pro</sup> can be explained by its pleotropic role. It was logical to assume that the viral protease is able to cleave not only viral substrates but also host proteins, adding to its complex role in infection. Recently, N-terminomics studies identified more than 100 M<sup>Pro</sup> substrates in human lung and kidney cells.<sup>32</sup> Gal-8—a host defense protein and one of the key regulators of immune response—was shown to be one of the host substrates. Gal-8 is responsible for secretion of cytokines and chemokines and involved in the development of cytokine storm, which was also reported for Gal-9<sup>67</sup>—a dangerous condition associated with more severe COVID-19 outcomes. In this study, we confirmed the cleavage of Gal-8 by M<sup>Pro</sup> and identified at least two additional cleavage sites by mass spectrometry—the one that was identified previously (Q158 in a linker region) and two additional sites at the termini, Q9 and Q248. The cleavage of Gal-8 by M<sup>Pro</sup> therefore follows more complex enzyme kinetics with several cleavage sites involved, some substrate products being intermediate (34 kDa and 21 kDa bands) and several products being stable after 24 h of cleavage, such as Gal-8<sup>10–158</sup> and Gal-8<sup>159–317</sup>. Interestingly, SARS-CoV M<sup>Pro</sup> demonstrated a similar pattern and rate for Gal-8 substrate cleavage. The stable cleavage product Gal-8<sup>159–317</sup> was monitored while comparing the activity among variants. Even though the difference in activity between M<sup>Pro</sup> variants toward Gal-8 was quite noticeable it remains to be determined how M<sup>Pro</sup> function relates to viral fitness and pathogenicity, and it is possible that in order to see the significant consequences for the host immune system the functionality of a variant's M<sup>Pro</sup> needs to be altered by a large amount. However, the known outcome of Gal-8 cleavage is the loss of ability to recruit the autophagy adaptor NDP52 to damaged endosomes, which allows SARS-CoV-2 to escape antiviral xenophagy. It was confirmed by immunoprecipitation that NDP52 binds the C-terminal domain of Gal-8 after its cleavage, but if Gal-8 is cleaved further at the newly identified Q246 site Gal-8 interaction with NDP52 might be also prevented.

In addition to the direct interaction of cytosolic Gal-8 with pathogen proteins, secreted Gal-8 also plays a role in the regulation of adaptive and innate immune responses by targeting cytokine receptors and inducing TNF signaling and cytokines and chemokines expression. Given the important role of Gal-8 in pathogenicity we sought to assess if M<sup>Pro</sup> cleavage affected the immunomodulatory properties of Gal-8. Interestingly, the cleavage products Gal-8<sup>10–158</sup> and Gal-8<sup>159–317</sup> still were able to enhance TNF- $\alpha$ /IL-6 expression in both PBMC culture and in CD14+ monocytes and B cells in vitro but with a less profound effect compared to the full-length of Gal-8, contributing to a decreased level of host

immunocompetence. Thus, the single event of M<sup>Pro</sup>-mediated cleavage of Gal-8 influences multiple ways for the virus to evade host defense pathways. First, intracellularly it defeats antiviral mechanism and allows SARS-CoV-2 to escape xenophagy, as it was demonstrated before,<sup>32</sup> and second once secreted the truncated form of Gal-8 causes a decreased immune response effect against viral infection. Further in vivo studies need to be performed to investigate the physiological effects of Gal-8 cleavage by different M<sup>Pro</sup> mutants and VOCs.

Lastly, emerging new variants cause a valid concern that COVID-19 might develop a resistance to known antivirals through mutation of vital amino acids residues in the active site important for drug binding. Importantly, despite some structural changes in substrate binding pockets for several mutants as well as alterations in  $K_M$  values for viral substrate we still observed maintained potency of nirmatrelvir and our derivative inhibitor against the variants of M<sup>Pro</sup>, suggesting M<sup>Pro</sup> remains an excellent antiviral target as the virus evolves. It also proves the concept of using protease inhibitors that fit within the substrate envelope which were validated to be less susceptible for drug resistance.<sup>63–65</sup>

As the COVID-19 pandemic continues to pose a global health threat with the increased ability of variants to spread and escape immune responses, SARS-CoV-2 antiviral drugs are necessary to combat the pandemic and to prevent future outbreaks. Potential drug resistance needs to be considered for the inhibitors targeting M<sup>Pro</sup> mutants with altered catalytic properties on viral and host substrates, so it is crucial to investigate the potency of existing antivirals. Future variants require close monitoring for possible drug resistance which needs to be considered for the development of next-generation M<sup>Pro</sup> inhibitors.

## ■ ASSOCIATED CONTENT

### Data Availability Statement

All data are available in the main text or the [Supporting Information](#). Inhibitors are available with materials transfer agreements (MTAs). Structural data have been deposited in the [www.rcsb.org](http://www.rcsb.org) database with accession numbers: 8DJJ.PDB M<sup>Pro</sup>-A7T; 8EJ9.PDB: M<sup>Pro</sup>-E47N; 8EJ7.PDB: M<sup>Pro</sup>-E47K; 8DKZ.PDB: M<sup>Pro</sup>-L50F; 8DKL.PDB: M<sup>Pro</sup>-L89F; 8DKJ.PDB: M<sup>Pro</sup>-K90R; 8DI3.PDB: M<sup>Pro</sup>-P132H; 8DK8.PDB: M<sup>Pro</sup>-T190L.

### SI Supporting Information

The Supporting Information is available free of charge at <https://pubs.acs.org/doi/10.1021/acscentsci.3c00054>.

Materials and methods include detailed experimental procedures about protein purifications, crystal structures analysis, size exclusion chromatography analysis, substrate specificity profiles, mass spectrometry analysis, galectins cleavage study, frequency of mutations study, crystallography data and refinement ([PDF](#))

Transparent Peer Review report available ([PDF](#))

## ■ AUTHOR INFORMATION

### Corresponding Author

M. Joanne Lemieux – Department of Biochemistry, University of Alberta, Edmonton, Alberta T6G 2H7, Canada; Li Ka Shing Institute of Virology, University of Alberta, Edmonton, Alberta T6G 2E1, Canada; [orcid.org/0000-0003-4745-9153](https://orcid.org/0000-0003-4745-9153); Email: [joanne.lemieux@ualberta.ca](mailto:joanne.lemieux@ualberta.ca)

## Authors

Sizhu Amelia Chen – Department of Biochemistry, University of Alberta, Edmonton, Alberta T6G 2H7, Canada; Li Ka Shing Institute of Virology, University of Alberta, Edmonton, Alberta T6G 2E1, Canada

Elena Arutyunova – Department of Biochemistry, University of Alberta, Edmonton, Alberta T6G 2H7, Canada; Li Ka Shing Institute of Virology, University of Alberta, Edmonton, Alberta T6G 2E1, Canada

Jimmy Lu – Department of Biochemistry, University of Alberta, Edmonton, Alberta T6G 2H7, Canada; Li Ka Shing Institute of Virology, University of Alberta, Edmonton, Alberta T6G 2E1, Canada

Muhammad Bashir Khan – Department of Biochemistry, University of Alberta, Edmonton, Alberta T6G 2H7, Canada

Wioletta Rut – Department of Chemical Biology and Bioimaging, Wrocław University of Science and Technology, Wrocław 50-370, Poland; [orcid.org/0000-0003-1261-5566](https://orcid.org/0000-0003-1261-5566)

Mikolaj Zmudzinski – Department of Chemical Biology and Bioimaging, Wrocław University of Science and Technology, Wrocław 50-370, Poland; [orcid.org/0000-0002-9792-9160](https://orcid.org/0000-0002-9792-9160)

Shima Shahbaz – Department of Dentistry & Dental Hygiene, University of Alberta, Edmonton, Alberta T6G 2E1, Canada

Jegan Iyyathurai – Department of Biochemistry, University of Alberta, Edmonton, Alberta T6G 2H7, Canada; Li Ka Shing Institute of Virology, University of Alberta, Edmonton, Alberta T6G 2E1, Canada

Eman W. Moussa – Department of Biochemistry, University of Alberta, Edmonton, Alberta T6G 2H7, Canada

Zoe Turner – Department of Biochemistry, University of Alberta, Edmonton, Alberta T6G 2H7, Canada; [orcid.org/0000-0002-3130-5208](https://orcid.org/0000-0002-3130-5208)

Bing Bai – Li Ka Shing Applied Virology Institute and Department of Medical Microbiology and Immunology, University of Alberta, Edmonton, Alberta T6G 2E1, Canada

Tess Lamer – Department of Chemistry, University of Alberta, Edmonton, Alberta T6G 2G2, Canada; [orcid.org/0000-0002-1511-4540](https://orcid.org/0000-0002-1511-4540)

James A. Nieman – Li Ka Shing Applied Virology Institute and Department of Medical Microbiology and Immunology, University of Alberta, Edmonton, Alberta T6G 2E1, Canada; [orcid.org/0000-0002-5087-0819](https://orcid.org/0000-0002-5087-0819)

John C. Vederas – Department of Chemistry, University of Alberta, Edmonton, Alberta T6G 2G2, Canada; [orcid.org/0000-0002-2996-0326](https://orcid.org/0000-0002-2996-0326)

Olivier Julien – Department of Biochemistry, University of Alberta, Edmonton, Alberta T6G 2H7, Canada; [orcid.org/0000-0001-7068-7299](https://orcid.org/0000-0001-7068-7299)

Marcin Drag – Department of Chemical Biology and Bioimaging, Wrocław University of Science and Technology, Wrocław 50-370, Poland; [orcid.org/0000-0001-8510-1967](https://orcid.org/0000-0001-8510-1967)

Shokrollah Elahi – Department of Dentistry & Dental Hygiene, University of Alberta, Edmonton, Alberta T6G 2E1, Canada; [orcid.org/0000-0002-7215-2009](https://orcid.org/0000-0002-7215-2009)

Howard S. Young – Department of Biochemistry, University of Alberta, Edmonton, Alberta T6G 2H7, Canada; [orcid.org/0000-0002-5990-8422](https://orcid.org/0000-0002-5990-8422)

Complete contact information is available at: <https://pubs.acs.org/doi/10.1021/acscentsci.3c00054>

## Author Contributions

Conceptualization: EA, SAC, JL, MJL. Methodology: SAC, JL, EA, MBK, JI, EM, WR, MZ, SS, ZT, BB, TL. Investigation: SAC, JL, MBK, JI, EM, MZ, WR, SS, ZT, BB, TL. Visualization: EA, SAC, JL. Supervision: JAN, OJ, SE, JN, MD, HSY, JCV, MJL. Writing: EA, SAC, JL. Writing-review and editing: SAC, EA, JL, MBK, WR, SS, JI, EM, ZT, BB.

## Funding

Canadian Institutes of Health Project Grant PJT 180390 Canadian Institutes of Health Research Rapid Research (VR3-172655). Natural Sciences and Engineering Research Council of Canada (549297-2019) Alberta Innovates Alberta Jobs, Economy and Innovation Infrastructure Grant - Government of Alberta Foundation for Polish Science

## Notes

The authors declare no competing financial interest.

## ACKNOWLEDGMENTS

We thank the staff at SSRL beamline 12-1, in particular Dr. Silvia Russi. Use of the Stanford Synchrotron Radiation Lightsource, SLAC National Accelerator Laboratory, is supported by the U.S. Department of Energy, Office of Science, Office of Basic Energy Sciences under Contract No. DE-AC02-76SF00515. The SSRL Structural Molecular Biology Program is supported by the DOE Office of Biological and Environmental Research, and by the National Institutes of Health, National Institute of General Medical Sciences (P30GM133894).

## ABBREVIATIONS

M<sup>pro</sup>, Main protease; Gal-8, Galectin-8

## REFERENCES

- (1) Lu, R.; Zhao, X.; Li, J.; Niu, P.; Yang, B.; Wu, H.; Wang, W.; Song, H.; Huang, B.; Zhu, N.; Bi, Y.; Ma, X.; Zhan, F.; Wang, L.; Hu, T.; Zhou, H.; Hu, Z.; Zhou, W.; Zhao, L.; Chen, J.; Meng, Y.; Wang, J.; Lin, Y.; Yuan, J.; Xie, Z.; Ma, J.; Liu, W. J.; Wang, D.; Xu, W.; Holmes, E. C.; Gao, G. F.; Wu, G.; Chen, W.; Shi, W.; Tan, W. Genomic characterisation and epidemiology of 2019 novel coronavirus: implications for virus origins and receptor binding. *Lancet* **2020**, *395* (10224), 565–574.
- (2) Hiscott, J.; Alexandridi, M.; Muscolini, M.; Tassone, E.; Palermo, E.; Soultioti, M.; Zevini, A. The global impact of the coronavirus pandemic. *Cytokine Growth Factor Rev.* **2020**, *53*, 1–9.
- (3) Bakhshandeh, B.; Jahanafrooz, Z.; Abbasi, A.; Goli, M. B.; Sadeghi, M.; Mottaqi, M. S.; Zamani, M. Mutations in SARS-CoV-2; Consequences in structure, function, and pathogenicity of the virus. *Microb Pathog* **2021**, *154*, 104831.
- (4) van Dorp, L.; Acman, M.; Richard, D.; Shaw, L. P.; Ford, C. E.; Ormond, L.; Owen, C. J.; Pang, J.; Tan, C. C. S.; Boshier, F. A. T.; Ortiz, A. T.; Balloux, F. Emergence of genomic diversity and recurrent mutations in SARS-CoV-2. *Infect Genet Evol* **2020**, *83*, 104351.
- (5) Khateeb, J.; Li, Y.; Zhang, H. Emerging SARS-CoV-2 variants of concern and potential intervention approaches. *Crit Care* **2021**, *25* (1), 244.
- (6) Fernandes, Q.; Inchakalody, V. P.; Merhi, M.; Mestiri, S.; Taib, N.; Moustafa Abo El-Ella, D.; Bedhiafi, T.; Raza, A.; Al-Zaidan, L.; Mohsen, M. O.; Yousuf Al-Nesf, M. A.; Hssain, A. A.; Yassine, H. M.; Bachmann, M. F.; Uddin, S.; Dermime, S. Emerging COVID-19 variants and their impact on SARS-CoV-2 diagnosis, therapeutics and vaccines. *Ann. Med.* **2022**, *54* (1), 524–540.
- (7) Zhou, W.; Wang, W. Fast-spreading SARS-CoV-2 variants: challenges to and new design strategies of COVID-19 vaccines. *Signal Transduct Target Ther* **2021**, *6* (1), 226.

- (8) Davies, N. G.; Abbott, S.; Barnard, R. C.; Jarvis, C. I.; Kucharski, A. J.; Munday, J. D.; Pearson, C. A. B.; Russell, T. W.; Tully, D. C.; Washburne, A. D.; Wenseleers, T.; Gimma, A.; Waite, W.; Wong, K. L. M.; van Zandvoort, K.; Silverman, J. D.; Diaz-Ordaz, K.; Keogh, R.; Eggo, R. M.; Funk, S.; Jit, M.; Atkins, K. E.; Edmunds, W. J. Estimated transmissibility and impact of SARS-CoV-2 lineage B.1.1.7 in England. *Science* **2021**, *372* (6538). DOI: 10.1126/science.abg3055
- (9) Lin, L.; Liu, Y.; Tang, X.; He, D. The Disease Severity and Clinical Outcomes of the SARS-CoV-2 Variants of Concern. *Front Public Health* **2021**, *9*, 775224.
- (10) Fontanet, A.; Autran, B.; Lina, B.; Kieny, M. P.; Karim, S. S. A.; Sridhar, D. SARS-CoV-2 variants and ending the COVID-19 pandemic. *Lancet* **2021**, *397* (10278), 952–954.
- (11) COVID-19: SARS-CoV-2 variant classifications and definitions. CDC. <https://www.cdc.gov/coronavirus/2019-ncov/variants/variant-classifications.html>.
- (12) Tracking SARS-CoV-2 variants. WHO, <https://www.who.int/activities/tracking-SARS-CoV-2-variants>.
- (13) Meredith, L. W.; Hamilton, W. L.; Warne, B.; Houldcroft, C. J.; Hosmillo, M.; Jahun, A. S.; Curran, M. D.; Parmar, S.; Caller, L. G.; Caddy, S. L.; Khokhar, F. A.; Yakovleva, A.; Hall, G.; Feltwell, T.; Forrest, S.; Sridhar, S.; Weekes, M. P.; Baker, S.; Brown, N.; Moore, E.; Popay, A.; Roddick, I.; Reacher, M.; Gouliouris, T.; Peacock, S. J.; Dougan, G.; Torok, M. E.; Goodfellow, I. Rapid implementation of SARS-CoV-2 sequencing to investigate cases of health-care associated COVID-19: a prospective genomic surveillance study. *Lancet Infect Dis* **2020**, *20* (11), 1263–1272.
- (14) Harvey, W. T.; Carabelli, A. M.; Jackson, B.; Gupta, R. K.; Thomson, E. C.; Harrison, E. M.; Ludden, C.; Reeve, R.; Rambaut, A.; Peacock, S. J.; Robertson, D. L. SARS-CoV-2 variants, spike mutations and immune escape. *Nat. Rev. Microbiol* **2021**, *19* (7), 409–424.
- (15) Wu, F.; Zhao, S.; Yu, B.; Chen, Y. M.; Wang, W.; Song, Z. G.; Hu, Y.; Tao, Z. W.; Tian, J. H.; Pei, Y. Y.; Yuan, M. L.; Zhang, Y. L.; Dai, F. H.; Liu, Y.; Wang, Q. M.; Zheng, J. J.; Xu, L.; Holmes, E. C.; Zhang, Y. Z. A new coronavirus associated with human respiratory disease in China. *Nature* **2020**, *579* (7798), 265–269.
- (16) Chen, Y.; Liu, Q.; Guo, D. Emerging coronaviruses: Genome structure, replication, and pathogenesis. *J. Med. Virol* **2020**, *92* (10), 2249.
- (17) Koyama, T.; Platt, D.; Parida, L. Variant analysis of SARS-CoV-2 genomes. *Bull. World Health Organ* **2020**, *98* (7), 495–504.
- (18) Korber, B.; Fischer, W. M.; Gnanakaran, S.; Yoon, H.; Theiler, J.; Abfalterer, W.; Hengartner, N.; Giorgi, E. E.; Bhattacharya, T.; Foley, B.; Hastie, K. M.; Parker, M. D.; Partridge, D. G.; Evans, C. M.; Freeman, T. M.; de Silva, T. I.; McDanal, C.; Perez, L. G.; Tang, H.; Moon-Walker, A.; Whelan, S. P.; LaBranche, C. C.; Saphire, E. O.; Montefiori, D. C.; Angyal, A.; Brown, R. L.; Carrilero, L.; Green, L. R.; Groves, D. C.; Johnson, K. J.; Keeley, A. J.; Lindsey, B. B.; Parsons, P. J.; Raza, M.; Rowland-Jones, S.; Smith, N.; Tucker, R. M.; Wang, D.; Wyles, M. D. Tracking Changes in SARS-CoV-2 Spike: Evidence that D614G Increases Infectivity of the COVID-19 Virus. *Cell* **2020**, *182* (4), 812–827.
- (19) Volz, E.; Hill, V.; McCrone, J. T.; Price, A.; Jorgensen, D.; O'Toole, A.; Southgate, J.; Johnson, R.; Jackson, B.; Nascimento, F. F.; Rey, S. M.; Nicholls, S. M.; Colquhoun, R. M.; da Silva Filipe, A.; Shephard, J.; Pascall, D. J.; Shah, R.; Jesudasan, N.; Li, K.; Jarrett, R.; Pacchiarini, N.; Bull, M.; Geidelberg, L.; Siveroni, I.; Consortium, C.-U.; Goodfellow, I.; Loman, N. J.; Pybus, O. G.; Robertson, D. L.; Thomson, E. C.; Rambaut, A.; Connor, T. R. Evaluating the Effects of SARS-CoV-2 Spike Mutation D614G on Transmissibility and Pathogenicity. *Cell* **2021**, *184* (1), 64–75.
- (20) Wibmer, C. K.; Ayres, F.; Hermanus, T.; Madzivhandila, M.; Kgagudi, P.; Oosthuysen, B.; Lambson, B. E.; de Oliveira, T.; Vermeulen, M.; van der Berg, K.; Rossouw, T.; Boswell, M.; Ueckermann, V.; Meiring, S.; von Gottberg, A.; Cohen, C.; Morris, L.; Bhiman, J. N.; Moore, P. L. SARS-CoV-2 501Y.V2 escapes neutralization by South African COVID-19 donor plasma. *Nat. Med.* **2021**, *27* (4), 622–625.



- (21) Yashvardhini, N.; Kumar, A.; Jha, D. K. Analysis of SARS-CoV-2 mutations in the main viral protease (NSP5) and its implications on the vaccine designing strategies. *Vacunas* **2022**, *23*, S1–S13.
- (22) Hilgenfeld, R. From SARS to MERS: crystallographic studies on coronaviral proteases enable antiviral drug design. *FEBS J.* **2014**, *281* (18), 4085–96.
- (23) Vuong, W.; Khan, M. B.; Fischer, C.; Arutyunova, E.; Lamer, T.; Shields, J.; Saffran, H. A.; McKay, R. T.; van Belkum, M. J.; Joyce, M. A.; Young, H. S.; Tyrrell, D. L.; Vederas, J. C.; Lemieux, M. J. Feline coronavirus drug inhibits the main protease of SARS-CoV-2 and blocks virus replication. *Nat. Commun.* **2020**, *11* (1), 4282.
- (24) Zhang, L.; Lin, D.; Sun, X.; Curth, U.; Drosten, C.; Sauerhering, L.; Becker, S.; Rox, K.; Hilgenfeld, R. Crystal structure of SARS-CoV-2 main protease provides a basis for design of improved alpha-ketoamide inhibitors. *Science* **2020**, *368* (6489), 409–412.
- (25) Arutyunova, E.; Khan, M. B.; Fischer, C.; Lu, J.; Lamer, T.; Vuong, W.; van Belkum, M. J.; McKay, R. T.; Tyrrell, D. L.; Vederas, J. C.; Young, H. S.; Lemieux, M. J. N-Terminal Finger Stabilizes the S1 Pocket for the Reversible Feline Drug GC376 in the SARS-CoV-2 M(pro) Dimer. *J. Mol. Biol.* **2021**, *433* (13), 167003.
- (26) Ivashkiv, L. B.; Donlin, L. T. Regulation of type I interferon responses. *Nat. Rev. Immunol.* **2014**, *14* (1), 36–49.
- (27) Zhu, X.; Fang, L.; Wang, D.; Yang, Y.; Chen, J.; Ye, X.; Foda, M. F.; Xiao, S. Porcine deltacoronavirus nsp5 inhibits interferon-beta production through the cleavage of NEMO. *Virology* **2017**, *502*, 33–38.
- (28) Zhu, X.; Chen, J.; Tian, L.; Zhou, Y.; Xu, S.; Long, S.; Wang, D.; Fang, L.; Xiao, S. Porcine Deltacoronavirus nsp5 Cleaves DCP1A To Decrease Its Antiviral Activity. *J. Virol.* **2020**, *94* (15). DOI: 10.1128/JVI.02162-19
- (29) Wang, D.; Fang, L.; Shi, Y.; Zhang, H.; Gao, L.; Peng, G.; Chen, H.; Li, K.; Xiao, S. Porcine Epidemic Diarrhea Virus 3C-Like Protease Regulates Its Interferon Antagonism by Cleaving NEMO. *J. Virol.* **2016**, *90* (4), 2090–101.
- (30) Chen, S.; Tian, J.; Li, Z.; Kang, H.; Zhang, J.; Huang, J.; Yin, H.; Hu, X.; Qu, L. Feline Infectious Peritonitis Virus Nsp5 Inhibits Type I Interferon Production by Cleaving NEMO at Multiple Sites. *Viruses* **2020**, *12* (1), 43.
- (31) Tribulatti, M. V.; Carabelli, J.; Prato, C. A.; Campetella, O. Galectin-8 in the onset of the immune response and inflammation. *Glycobiology* **2020**, *30* (3), 134–142.
- (32) Pablos, I.; Machado, Y.; de Jesus, H. C. R.; Mohamud, Y.; Kappelhoff, R.; Lindskog, C.; Vlok, M.; Bell, P. A.; Butler, G. S.; Grin, P. M.; Cao, Q. T.; Nguyen, J. P.; Solis, N.; Abbina, S.; Rut, W.; Vederas, J. C.; Szekely, L.; Szakos, A.; Drag, M.; Kizhakkedathu, J. N.; Mossman, K.; Hirota, J. A.; Jan, E.; Luo, H.; Banerjee, A.; Overall, C. M. Mechanistic insights into COVID-19 by global analysis of the SARS-CoV-2 3CL(pro) substrate degradome. *Cell Rep* **2021**, *37* (4), 109892.
- (33) Zick, Y. Galectin-8, cytokines, and the storm. *Biochem. Soc. Trans.* **2022**, *50* (1), 135–149.
- (34) Bell, S. L.; Lopez, K. L.; Cox, J. S.; Patrick, K. L.; Watson, R. O. Galectin-8 Senses Phagosomal Damage and Recruits Selective Autophagy Adapter TAX1BP1 To Control Mycobacterium tuberculosis Infection in Macrophages. *mBio* **2021**, *12* (4), e0187120.
- (35) Thurston, T. L.; Wandel, M. P.; von Muhlinen, N.; Foeglein, A.; Randow, F. Galectin 8 targets damaged vesicles for autophagy to defend cells against bacterial invasion. *Nature* **2012**, *482* (7385), 414–8.
- (36) Hu, J.; Peng, P.; Cao, X.; Wu, K.; Chen, J.; Wang, K.; Tang, N.; Huang, A. L. Increased immune escape of the new SARS-CoV-2 variant of concern Omicron. *Cell Mol. Immunol.* **2022**, *19* (2), 293–295.
- (37) Owen, D. R.; Allerton, C. M. N.; Anderson, A. S.; Aschenbrenner, L.; Avery, M.; Berritt, S.; Boras, B.; Cardin, R. D.; Carlo, A.; Coffman, K. J.; Dantonio, A.; Di, L.; Eng, H.; Ferre, R.; Gajiwala, K. S.; Gibson, S. A.; Greasley, S. E.; Hurst, B. L.; Kadar, E. P.; Kalgutkar, A. S.; Lee, J. C.; Lee, J.; Liu, W.; Mason, S. W.; Noell, S.; Novak, J. J.; Obach, R. S.; Ogilvie, K.; Patel, N. C.; Pettersson, M.; Rai, D. K.; Reese, M. R.; Sammons, M. F.; Sathish, J. G.; Singh, R. S. P.; Steppan, C. M.; Stewart, A. E.; Tuttle, J. B.; Updyke, L.; Verhoest, P. R.; Wei, L.; Yang, Q.; Zhu, Y. An oral SARS-CoV-2 M(pro) inhibitor clinical candidate for the treatment of COVID-19. *Science* **2021**, *374* (6575), 1586–1593.
- (38) Pfizer Receives U.S. FDA Emergency Use Authorization for Novel COVID-19 Oral Antiviral Treatment. Pfizer, <https://www.pfizer.com/news/press-release/press-release-detail/pfizer-receives-us-fda-emergency-use-authorization-novel>.
- (39) Lu, J.; Chen, S. A.; Khan, M. B.; Brassard, R.; Arutyunova, E.; Lamer, T.; Vuong, W.; Fischer, C.; Young, H. S.; Vederas, J. C.; Lemieux, M. J. Crystallization of Feline Coronavirus M(pro) With GC376 Reveals Mechanism of Inhibition. *Front Chem.* **2022**, *10*, 852210.
- (40) Vuong, W.; Fischer, C.; Khan, M. B.; van Belkum, M. J.; Lamer, T.; Willoughby, K. D.; Lu, J.; Arutyunova, E.; Joyce, M. A.; Saffran, H. A.; Shields, J. A.; Young, H. S.; Nieman, J. A.; Tyrrell, D. L.; Lemieux, M. J.; Vederas, J. C. Improved SARS-CoV-2 M(pro) inhibitors based on feline antiviral drug GC376: Structural enhancements, increased solubility, and micellar studies. *Eur. J. Med. Chem.* **2021**, *222*, 113584.
- (41) Bai, B.; Arutyunova, E.; Khan, M. B.; Lu, J.; Joyce, M. A.; Saffran, H. A.; Shields, J. A.; Kandadai, A. S.; Belovodskiy, A.; Hena, M.; Vuong, W.; Lamer, T.; Young, H. S.; Vederas, J. C.; Tyrrell, D. L.; Lemieux, M. J.; Nieman, J. A. Peptidomimetic nitrile warheads as SARS-CoV-2 3CL protease inhibitors. *RSC Med. Chem.* **2021**, *12* (10), 1722–1730.
- (42) Bai, B.; Belovodskiy, A.; Hena, M.; Kandadai, A. S.; Joyce, M. A.; Saffran, H. A.; Shields, J. A.; Khan, M. B.; Arutyunova, E.; Lu, J.; Bajwa, S. K.; Hockman, D.; Fischer, C.; Lamer, T.; Vuong, W.; van Belkum, M. J.; Gu, Z.; Lin, F.; Du, Y.; Xu, J.; Rahim, M.; Young, H. S.; Vederas, J. C.; Tyrrell, D. L.; Lemieux, M. J.; Nieman, J. A. Peptidomimetic alpha-Acyloxymethylketone Warheads with Six-Membered Lactam P1 Glutamine Mimic: SARS-CoV-2 3CL Protease Inhibition, Coronavirus Antiviral Activity, and in Vitro Biological Stability. *J. Med. Chem.* **2022**, *65* (4), 2905–2925.
- (43) Abe, K.; Kabe, Y.; Uchiyama, S.; Iwasaki, Y. W.; Ishizu, H.; Uwamino, Y.; Takenouchi, T.; Uno, S.; Ishii, M.; Maruno, T.; Noda, M.; Murata, M.; Hasegawa, N.; Saya, H.; Kitagawa, Y.; Fukunaga, K.; Amagai, M.; Siomi, H.; Suematsu, M.; Kosaki, K.; Keio Donner, P. Pro108Ser mutation of SARS-CoV-2 3CL(pro) reduces the enzyme activity and ameliorates the clinical severity of COVID-19. *Sci. Rep.* **2022**, *12* (1), 1299.
- (44) Sacco, M. D.; Hu, Y.; Gongora, M. V.; Meilleur, F.; Kemp, M. T.; Zhang, X.; Wang, J.; Chen, Y. The P132H mutation in the main protease of Omicron SARS-CoV-2 decreases thermal stability without compromising catalysis or small-molecule drug inhibition. *Cell Res.* **2022**, *32* (5), 498–500.
- (45) Jin, Z.; Du, X.; Xu, Y.; Deng, Y.; Liu, M.; Zhao, Y.; Zhang, B.; Li, X.; Zhang, L.; Peng, C.; Duan, Y.; Yu, J.; Wang, L.; Yang, K.; Liu, F.; Jiang, R.; Yang, X.; You, T.; Liu, X.; Yang, X.; Bai, F.; Liu, H.; Liu, X.; Guddat, L. W.; Xu, W.; Xiao, G.; Qin, C.; Shi, Z.; Jiang, H.; Rao, Z.; Yang, H. Structure of M(pro) from SARS-CoV-2 and discovery of its inhibitors. *Nature* **2020**, *582* (7811), 289–293.
- (46) Pillaiyar, T.; Manickam, M.; Namasivayam, V.; Hayashi, Y.; Jung, S. H. An Overview of Severe Acute Respiratory Syndrome-Coronavirus (SARS-CoV) 3CL Protease Inhibitors: Peptidomimetics and Small Molecule Chemotherapy. *J. Med. Chem.* **2016**, *59* (14), 6595–628.
- (47) Rut, W.; Groborz, K.; Zhang, L.; Sun, X.; Zmudzinski, M.; Pawlik, B.; Wang, X.; Jochmans, D.; Neyts, J.; Mlynarski, W.; Hilgenfeld, R.; Drag, M. SARS-CoV-2 M(pro) inhibitors and activity-based probes for patient-sample imaging. *Nat. Chem. Biol.* **2021**, *17* (2), 222–228.
- (48) Tandel, D.; Sah, V.; Singh, N. K.; Potharaju, P. S.; Gupta, D.; Shrivastava, S.; Sowpati, D. T.; Harshan, K. H. SARS-CoV-2 Variant Delta Potently Suppresses Innate Immune Response and Evades Interferon-Activated Antiviral Responses in Human Colon Epithelial Cells. *Microbiology Spectrum* **2022**, *10* (5), e0160422.

- (49) Chen, G.; Wu, D.; Guo, W.; Cao, Y.; Huang, D.; Wang, H.; Wang, T.; Zhang, X.; Chen, H.; Yu, H.; Zhang, X.; Zhang, M.; Wu, S.; Song, J.; Chen, T.; Han, M.; Li, S.; Luo, X.; Zhao, J.; Ning, Q. Clinical and immunological features of severe and moderate coronavirus disease 2019. *J. Clin. Invest.* **2020**, *130* (5), 2620–2629.
- (50) Teysou, E.; Delagrèverie, H.; Visseaux, B.; Lambert-Niclot, S.; Briclher, S.; Ferre, V.; Marot, S.; Jary, A.; Todesco, E.; Schnuriger, A.; Ghidaoui, E.; Abdi, B.; Akhavan, S.; Houhou-Fidouh, N.; Charpentier, C.; Morand-Joubert, L.; Boutolleau, D.; Descamps, D.; Calvez, V.; Marcelin, A. G.; Soulie, C. The Delta SARS-CoV-2 variant has a higher viral load than the Beta and the historical variants in nasopharyngeal samples from newly diagnosed COVID-19 patients. *Journal of Infection* **2021**, *83* (4), e1–e3.
- (51) Singanayagam, A.; Hakki, S.; Dunning, J.; Madon, K. J.; Crone, M. A.; Koycheva, A.; Derqui-Fernandez, N.; Barnett, J. L.; Whitfield, M. G.; Varro, R.; Charlett, A.; Kundu, R.; Fenn, J.; Cutajar, J.; Quinn, V.; Conibear, E.; Barclay, W.; Freemont, P. S.; Taylor, G. P.; Ahmad, S.; Zambon, M.; Ferguson, N. M.; Lalvani, A. Community transmission and viral load kinetics of the SARS-CoV-2 delta (B.1.617.2) variant in vaccinated and unvaccinated individuals in the UK: a prospective, longitudinal, cohort study. *The Lancet. Infectious Diseases* **2022**, *22* (2), 183–195.
- (52) Hu, T.; Zhang, Y.; Li, L.; Wang, K.; Chen, S.; Chen, J.; Ding, J.; Jiang, H.; Shen, X. Two adjacent mutations on the dimer interface of SARS coronavirus 3C-like protease cause different conformational changes in crystal structure. *Virology* **2009**, *388* (2), 324–34.
- (53) Chen, S.; Zhang, J.; Hu, T.; Chen, K.; Jiang, H.; Shen, X. Residues on the dimer interface of SARS coronavirus 3C-like protease: dimer stability characterization and enzyme catalytic activity analysis. *Journal of Biochemistry* **2007**, *143* (4), 525–36.
- (54) Chen, S.; Hu, T.; Zhang, J.; Chen, J.; Chen, K.; Ding, J.; Jiang, H.; Shen, X. Mutation of Gly-11 on the dimer interface results in the complete crystallographic dimer dissociation of severe acute respiratory syndrome coronavirus 3C-like protease: crystal structure with molecular dynamics simulations. *J. Biol. Chem.* **2008**, *283* (1), 554–564.
- (55) Blanchard, J. E.; Elowe, N. H.; Huitema, C.; Fortin, P. D.; Cechetto, J. D.; Eltis, L. D.; Brown, E. D. High-throughput screening identifies inhibitors of the SARS coronavirus main proteinase. *Chemistry & Biology* **2004**, *11* (10), 1445–53.
- (56) Shaqra, A. M.; Zvornicanin, S. N.; Huang, Q. Y. J.; Lockbaum, G. J.; Knapp, M.; Tandeske, L.; Bakan, D. T.; Flynn, J.; Bolon, D. N. A.; Moquin, S.; Dovala, D.; Kurt Yilmaz, N.; Schiffer, C. A. Defining the substrate envelope of SARS-CoV-2 main protease to predict and avoid drug resistance. *Nat. Commun.* **2022**, *13* (1), 3556.
- (57) Lee, J.; Kenward, C.; Worrall, L. J.; Vuckovic, M.; Gentile, F.; Ton, A. T.; Ng, M.; Cherkasov, A.; Strynadka, N. C. J.; Paetzel, M. X-ray crystallographic characterization of the SARS-CoV-2 main protease polypeptide cleavage sites essential for viral processing and maturation. *Nat. Commun.* **2022**, *13* (1), 5196.
- (58) Lee, J.; Worrall, L. J.; Vuckovic, M.; Rosell, F. I.; Gentile, F.; Ton, A. T.; Caveney, N. A.; Ban, F.; Cherkasov, A.; Paetzel, M.; Strynadka, N. C. J. Crystallographic structure of wild-type SARS-CoV-2 main protease acyl-enzyme intermediate with physiological C-terminal autoprocessing site. *Nat. Commun.* **2020**, *11* (1), 5877.
- (59) Sacco, M. D.; Ma, C.; Lagarias, P.; Gao, A.; Townsend, J. A.; Meng, X.; Dube, P.; Zhang, X.; Hu, Y.; Kitamura, N.; Hurst, B.; Tarbet, B.; Marty, M. T.; Kolocouris, A.; Xiang, Y.; Chen, Y.; Wang, J. Structure and inhibition of the SARS-CoV-2 main protease reveal strategy for developing dual inhibitors against M(pro) and cathepsin L. *Sci. Adv.* **2020**, *6* (50). DOI: 10.1126/sciadv.abe0751
- (60) Muramatsu, T.; Takemoto, C.; Kim, Y. T.; Wang, H.; Nishii, W.; Terada, T.; Shirouzu, M.; Yokoyama, S. SARS-CoV 3CL protease cleaves its C-terminal autoprocessing site by novel subsite cooperativity. *Proc. Natl. Acad. Sci. U. S. A.* **2016**, *113* (46), 12997–13002.
- (61) Shi, J.; Sivaraman, J.; Song, J. Mechanism for controlling the dimer-monomer switch and coupling dimerization to catalysis of the severe acute respiratory syndrome coronavirus 3C-like protease. *J. Virol.* **2008**, *82* (9), 4620–9.
- (62) Kang, X.; Zhong, N.; Zou, P.; Zhang, S.; Jin, C.; Xia, B. Foldon unfolding mediates the interconversion between M(pro)-C monomer and 3D domain-swapped dimer. *Proc. Natl. Acad. Sci. U. S. A.* **2012**, *109* (37), 14900–5.
- (63) Prabu-Jeyabalan, M.; Nalivaika, E.; Schiffer, C. A. Substrate shape determines specificity of recognition for HIV-1 protease: analysis of crystal structures of six substrate complexes. *Structure* **2002**, *10*, 369–381a.
- (64) Shen, Y.; Altman, M. D.; Ali, A.; Nalam, M. N.; Cao, H.; Rana, T. M.; Schiffer, C. A.; Tidor, B. Testing the substrate-envelope hypothesis with designed pairs of compounds. *ACS Chem. Biol.* **2013**, *8* (11), 2433–2441.
- (65) Romano, K. P.; Ali, A.; Aydin, C.; Soumana, D.; Ozen, A.; Deveau, L. M.; Silver, C.; Cao, H.; Newton, A.; Petropoulos, C. J.; Huang, W.; Schiffer, C. A. The molecular basis of drug resistance against hepatitis C virus NS3/4A protease inhibitors. *PLoS pathogens* **2012**, *8* (7), e1002832.
- (66) Gunther, S.; Reinke, P. Y. A.; Fernandez-Garcia, Y.; Lieske, J.; Lane, T. J.; Ginn, H. M.; Koua, F. H. M.; Ehrt, C.; Ewert, W.; Oberthuer, D.; Yefanov, O.; Meier, S.; Lorenzen, K.; Krichel, B.; Kopicki, J. D.; Gelisio, L.; Brehm, W.; Dunkel, I.; Seychell, B.; Gieseler, H.; Norton-Baker, B.; Escudero-Perez, B.; Domaracký, M.; Saouane, S.; Tolstikova, A.; White, T. A.; Hanle, A.; Groessler, M.; Fleckenstein, H.; Trost, F.; Galchenkova, M.; Gevorgov, Y.; Li, C.; Awel, S.; Peck, A.; Barthelmess, M.; Schlunzen, F.; Lourdu Xavier, P.; Werner, N.; Andaleeb, H.; Ullah, N.; Falke, S.; Srinivasan, V.; Franca, B. A.; Schwinzer, M.; Brognaro, H.; Rogers, C.; Melo, D.; Zaitseva-Doyle, J. J.; Knoska, J.; Pena-Murillo, G. E.; Mashhour, A. R.; Hennicke, V.; Fischer, P.; Hakanpaa, J.; Meyer, J.; Gribbon, P.; Ellinger, B.; Kuzikov, M.; Wolf, M.; Beccari, A. R.; Bourenkov, G.; von Stetten, D.; Pompidor, G.; Bento, I.; Panneerselvam, S.; Karpics, I.; Schneider, T. R.; Garcia-Alai, M. M.; Niebling, S.; Gunther, C.; Schmidt, C.; Schubert, R.; Han, H.; Boger, J.; Monteiro, D. C. F.; Zhang, L.; Sun, X.; Pletzer-Zelgert, J.; Wollenhaupt, J.; Feiler, C. G.; Weiss, M. S.; Schulz, E. C.; Mehrabi, P.; Karnicar, K.; Usenik, A.; Loboda, J.; Tidow, H.; Chari, A.; Hilgenfeld, R.; Uetrecht, C.; Cox, R.; Zaliani, A.; Beck, T.; Rarey, M.; Gunther, S.; Turk, D.; Hinrichs, W.; Chapman, H. N.; Pearson, A. R.; Betzel, C.; Meents, S. A. X-ray screening identifies active site and allosteric inhibitors of SARS-CoV-2 main protease. *Science* **2021**, *372* (6542), 642–646.
- (67) Bozorgmehr, N.; Mashhour, S.; Perez Rosero, E.; Xu, L.; Shahbaz, S.; Sligl, W.; Osman, M.; Kutsogiannis, D. J.; MacIntyre, E.; O’Neil, C. R.; Elahi, S. Galectin-9, a Player in Cytokine Release Syndrome and a Surrogate Diagnostic Biomarker in SARS-CoV-2 Infection. *mBio* **2021**, *12* (3). DOI: 10.1128/mBio.00384-21